Evaluation of Tropospheric Water Vapor Simulations from the Atmospheric Model Intercomparison Project

DIAN J. GAFFEN

NOAA/Environmental Research Laboratories, Air Resources Laboratory, Silver Spring, Maryland

RICHARD D. ROSEN AND DAVID A. SALSTEIN

Atmospheric and Environmental Research, Inc., Cambridge, Massachusetts

JAMES S. BOYLE

Program for Climate Model Diagnosis and Intercomparison, Lawrence Livermore National Laboratory, Livermore, California

(Manuscript received 3 May 1996, in final form 8 November 1996)

ABSTRACT

Simulations of humidity from 28 general circulation models for the period 1979–88 from the Atmospheric Model Intercomparison Project are compared with observations from radiosondes over North America and the globe and with satellite microwave observations over the Pacific basin. The simulations of decadal mean values of precipitable water (W) integrated over each of these regions tend to be less moist than the real atmosphere in all three cases; the median model values are approximately 5% less than the observed values.

The spread among the simulations is larger over regions of high terrain, which suggests that differences in methods of resolving topographic features are important. The mean elevation of the North American continent is substantially higher in the models than is observed, which may contribute to the overall dry bias of the models over that area. The authors do not find a clear association between the mean topography of a model and its mean W simulation, however, which suggests that the bias over land is not purely a matter of orography.

The seasonal cycle of W is reasonably well simulated by the models, although over North America they have a tendency to become moister more quickly in the spring than is observed. The interannual component of the variability of W is not well captured by the models over North America. Globally, the simulated W values show a signal correlated with the Southern Oscillation index but the observations do not. This discrepancy may be related to deficiencies in the radiosonde network, which does not sample the tropical ocean regions well. Overall, the interannual variability of W, as well as its climatology and mean seasonal cycle, are better described by the median of the 28 simulations than by individual members of the ensemble.

Tests to learn whether simulated precipitable water, evaporation, and precipitation values may be related to aspects of model formulation yield few clear signals, although the authors find, for example, a tendency for the few models that predict boundary layer depth to have large values of evaporation and precipitation. Controlled experiments, in which aspects of model architecture are systematically varied within individual models, may be necessary to elucidate whether and how model characteristics influence simulations.

1. Introduction

Water vapor and the processes that control its abundance in the troposphere play a major role in the global climate system. The condensation of water vapor, for example, with its attendant release of latent heat, provides much of the energy to drive the atmosphere's circulation. Water vapor also strongly modulates the transfer of radiation within the atmosphere and so, through this process as well, influences the overall energy balance of the planet. Finally, with its great mobility and brief atmospheric residence time, water vapor is a central component of the global hydrological cycle.

Because of the importance of water vapor in the climate system, and, presumably, in climate models, a number of assessments of simulations of humidity by general circulation models (GCMs) have been performed. Rind et al. (1991) and Del Genio et al. (1994) compared satellite observations of upper-tropospheric humidity with simulations by the GISS GCM. (See Table 1 for model abbreviations.) Gaffen and Barnett (1992) compared interannual variations of specific humidity from radiosonde observations with simulations from the University of Hamburg version of the ECMWF GCM, and Chen et al. (1996) compared a more recent version of that model with satellite-derived estimates of

Corresponding author address: Dr. Dian J. Gaffen, NOAA (R/E/AR), 1315 East–West Highway, Silver Spring, MD 20910.
E-mail: Dian.Gaffen@noaa.gov

TABLE 1. Model abbreviations.

BMRC	Bureau of Meteorology Research Centre, Australia
CCC	Canadian Centre for Climate Research
CNRM	Centre Nationale de Recherches Météorologiques, France
COLA	Center for Ocean–Land–Atmosphere Studies
CSIRO	Commonwealth Scientific and Industrial Research Organization, Australia
CSU	Colorado State University
DERF	Dynamical Extended Range Forecasting (GFDL)
DNM	Department of Numerical Mathematics of the Russian Academy of Sciences
ECMWF	European Centre for Medium-Range Weather Forecasts
GFDL	Geophysical Fluid Dynamics Laboratory
GISS	Goddard Institute for Space Studies
GLA	Goddard Laboratory for Atmospheres
GSFC	Goddard Space Flight Center
JMA	Japan Meteorological Agency
LMD	Laboratoire de Météorologie Dynamique, France
MGO	Main Geophysical Observatory, Russia
MPI	Max-Planck-Institut für Meteorologie, Germany
MRI	Meteorological Research Institute, Japan
NCAR	National Center for Atmospheric Research
NMC	National Meteorological Center (now the National Centers for Environmental Prediction)
NRL	Naval Research Laboratory
SNG	SUNYA/NCAR Genesis model
SUNYA	State University of New York at Albany
UCLA	University of California, Los Angeles
UGAMP	Universities Global Atmospheric Modelling Programme, United Kingdom
UIUC	University of Illinois at Urbana-Champaign
UKMO	U.K. Meteorological Office
YONU	Yonsei University, Korea

precipitable water and upper-tropospheric relative humidity. Roads et al. (1992) compared the Los Alamos GCM with NMC analyses of water vapor, water vapor flux, and water vapor flux divergence. Boyle (1993) and Phillips et al. (1995) examined the effect of horizontal resolution in the ECMWF model on precipitable water, among other things. Soden and Bretherton (1994) compared the ECMWF and NCAR GCMs' precipitable water and upper-tropospheric humidity fields with operational analyses and with satellite observations. Bony and Duvel (1994) and Bony et al. (1995) used satellite observations and ECMWF analyses of precipitable water to evaluate the LMD GCM for the period of the Atmospheric Model Intercomparison Project (AMIP), and Salathé et al. (1995) compared GLA model simulations of upper-tropospheric humidity for the AMIP with satellite observations. Thompson and Pollard (1995) compared satellite-derived observations of precipitable water with simulations by the SNG model, and Roads et al. (1996) compared NMC analyses of precipitable water and moisture flux convergence with climatological fields from the NCAR GCM.

While shedding light on aspects of particular models' humidity simulations, these studies do not give a broader sense of the state of the science in the ability of GCMs to model humidity and moisture flux fields. The Atmospheric Model Intercomparison Project has provided an opportunity to compare systematically various aspects of many GCM humidity simulations with observations. Here, we compare humidity and meridional moisture flux simulations produced for the AMIP with observations to evaluate GCM simulations of both the climatology and the seasonal and interannual variability of tropospheric water vapor.

2. The Atmospheric Model Intercomparison Project

A project of the World Meteorological Organization's World Climate Research Programme, the AMIP is an international effort to evaluate the ability of atmospheric GCMs to simulate the global climate of the decade 1979–88 (Gates 1992). The 30 participating modeling groups followed a common experimental plan that involved using identical model boundary conditions of observed monthly mean sea surface temperature and sea ice, a constant concentration of atmospheric carbon dioxide (345 ppm), and a solar constant of 1365 W m^{-2}. Model output was provided for a specified set of fields in a standard format.

Twenty-five diagnostic subprojects have been examining various aspects of the simulations. This paper reports on some of the work of AMIP Diagnostic Subproject 11, entitled ''Validation of Humidity, Moisture Fluxes, and Soil Moisture in GCMs.'' Results concerning soil moisture are reported by Robock et al. (1995). Other AMIP results related to the hydrological cycle can be found in the following studies: Lau et al. (1995) on precipitation and evaporation, Duvel et al. (1997) on the clear-sky greenhouse effect of water vapor and the distribution of water vapor over ocean regions, Weare et al. (1995) on cloudiness, and Srinivasan et al. (1995) on tropical precipitation.

This study involves several AMIP monthly mean standard output fields: gridded precipitable water W, evaporation E, precipitation P, and zonal-mean specific humidity q. We were unable to examine relative humidity simulations because gridded relative humidity fields were not required as standard output. The availability of monthly mean values directed our attention to seasonal and longer timescales. We analyzed output from 28 of the AMIP models, listed in Table 1, that passed the quality control tests made at Lawrence Livermore National Laboratory by the Program for Climate Model Diagnosis and Intercomparison, which is responsible for AMIP coordination.

Because water vapor is a short-lived atmospheric constituent with high spatial and temporal variability, its distribution is particularly difficult to measure. Therefore, a reliable global water vapor dataset for model evaluation over the AMIP decade is not available. Over land, radiosonde data are most useful, despite their known shortcomings (Elliott and Gaffen 1991; Soden and Lanzante 1996). Over ocean, where surface micro-

wave emissions are reasonably homogeneous, satellite microwave measurements are becoming suitable but are not available for all years of the AMIP decade. We used different observational datasets for three different regions, and we will present our results for each in the following three sections. We discuss first the results for North America, where our observational data are plentiful and most reliable. Then, we examine a region of the atmosphere with a different underlying surface: the Pacific Ocean. Third, we follow with a look at the global scale.

3. Precipitable water over North America

a. North American radiosonde data

Our best verification data for the AMIP period are radiosonde observations over the North American continent. We used a dense and homogeneous network of 129 stations, depicted in Fig. 1a, in Canada, the United States, and Mexico, most of which used the VIZ radiosonde (Gaffen 1993, 1996). Daily soundings for the AMIP period (1979–88) were used to create monthly means of W, the integral of specific humidity with respect to pressure, in the column from the surface to 300 hPa, at each station. [Details about the data processing can be found in Ross and Elliott (1996a,b).] Monthly values were accepted only if at least 10 days of data were available for the month.

The station monthly mean data were then interpolated onto a 4° lat × 4° long grid (Fig. 1a). Gridpoint values were computed as a simple linear, distance-weighted average of observations from all stations within a radius of 2° lat of the grid point. To ensure the representativeness of gridded climatological values for the 10-yr period, a nearby station needed to report at least 9 of the 10 possible values for each calendar month for each grid box. For this spatial resolution, the radiosonde network samples Mexico and the United States quite well; typically about 95% of the grid boxes in each zonal band have stations within the specified radius. Poleward of 50°N sampling is worse—the comparable statistic is about 75%—in part because of the sparser network but also because of missing humidity data at 300 hPa in winter.

Examination of the data for both 0000 and 1200 UTC showed that, over most of the continent, the observed climatology of precipitable water is only minimally affected by choice of observation time. The North American decadal mean W for 0000 and 1200 UTC differs by less than 1%. Only over Mexico are the 0000 and 1200 UTC monthly means noticeably different, probably because some Mexican stations did not make 0000 UTC observations during the latter years of the period. Therefore, we chose to analyze North American 1200 UTC monthly means only. The monthly means for the models, however, were based on at least four samples per simulated day.

For comparison, model W fields over continental North America were regridded to the same 4° resolution as the observations. The observed and modeled monthly means were used to create 10-yr mean values for each calendar month, and monthly and seasonal anomalies were defined as the difference between a given value and the 10-yr mean for the appropriate month or season.

b. Climatological precipitable water

Figure 1 shows the observed and simulated climatologies of W over North America, namely, observed decadal mean values (Fig. 1a) and the median of the decadal mean simulations for the 28 models (Fig. 1b). Throughout this paper, we use the median as a measure of central tendencies of the GCM simulations because it is robust (in dealing with a non-Gaussian distribution) and resistant (to outliers). Likewise, we use the interquartile range (IQR; the difference between the upper- and lower-quartile values) as a robust and resistant measure of the spread among the 28 simulations. [See Wilks (1995) for a recent discussion of these statistics.]

As expected, both the observations (Fig. 1a) and simulations (Fig. 1b) show a general decrease of W with latitude and lower W values over the high terrain of the western mountains. The differences between the median of the model simulations and the observations (Fig. 1c) are small relative to either value and are generally less than 2 mm. As indicated in Fig. 1c, the models tend to be slightly moister than observed in the central and northeastern parts of the continent, and slightly drier than observed over western North America and the southeastern United States.

1) CONTINENTAL AVERAGES

To facilitate intermodel comparison, we examined the average W for the entire continent for the entire AMIP decade. The observations were averaged using the gridded data and assigning the appropriate zonal average value to any land grid boxes without data (see Fig. 1a). Spatial averages for the simulations were computed using all available continental values and the land masks appropriate to each model. Offshore island regions were excluded from the continental averages.

Figure 2 shows the observed mean North American W value of 15.2 mm (1 mm = 1 kg m^{-2}) and values for each of the 28 models. The median value from the models is 14.5 mm, 5% less than observed, and is shown in the box plot, which, following Tukey (1977), also gives the 25th and 75th percentile values (and thus the IQR) and the minimum and maximum values. The IQR of model values is 1.4 mm, about 10% of the median value; the full range is 3.6 mm.

We note that the minimum observed annual mean North American W is 14.8 mm (for 1979) and that fully half the models never achieve an annual mean value as

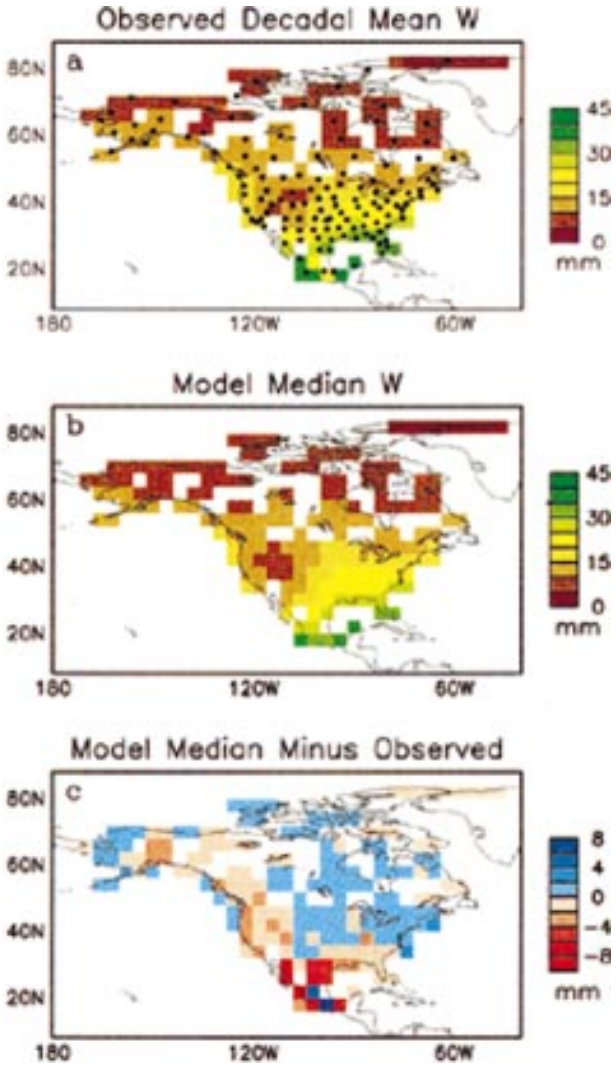

FIG. 1. (a) Decadal mean *W* as observed over North America and the locations of radiosonde stations for which data were used in this part of the study. (b) Median values of 28 model simulations of the decadal mean *W* at the locations of the observations. (c) The difference between the model median and observed fields.

large as this during any of the 10 yr of the simulations. This lack of overlap in the annual results suggests that the differences between the models and the observation are significant. By the same token, three models had all 10 annual mean values higher than the maximum observed annual mean of 15.6 mm (for 1986).

The extreme model mean values are from the SUNYA and NCAR models (Fig. 2), which represent successive generations of the Community Climate Model. This indicates that models derived from the same original code can produce highly dissimilar results.

2) TOPOGRAPHY AND PRECIPITABLE WATER

Because *W* is a column-integrated quantity, and because water vapor content decreases rapidly with height,

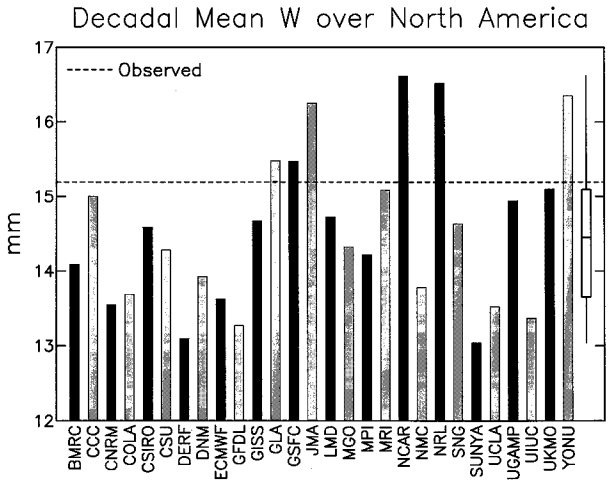

FIG. 2. Decadal mean *W* averaged over North America from 28 AMIP models (bars) and as observed by radiosondes (dashed line). The box plot at right gives the distribution of model values including the minimum, 25th, 50th, and 75th percentile, and maximum values.

surface topography has a strong influence on *W*, which may provide a possible explanation for the dry bias in many of the models. The average elevation of the North American continent, as ''sampled'' by the 129-station radiosonde network (Fig. 1a), is 290 m. For the 24 GCMs with available surface elevation data, the mean North American elevation ranged from 470 to 886 m, with a median value of 556 m. The discrepancy between the radiosonde network mean elevation and those of the GCMs is due, in part, to the tendency for radiosonde stations to be located in low elevation areas, and, in part, to the enhancement of orography in five of the GCMs (Phillips 1994). Thus the models are ''missing'' about 270 m of the planetary boundary layer, which could account for about 1 mm of precipitable water.

We cannot explain each model's individual bias, however, by invoking topographic considerations. Thus, it is not the case that the driest models have the highest mean elevations. In fact, there is no significant correlation between mean model elevation and decadal mean *W* over North America.

3) ZONAL AVERAGES

To summarize the models' performance as a function of latitude, we examined the zonal and decadal mean precipitable water over North America. Figure 3 shows the distribution of the models' meridional profiles of *W*, in zonal bands of 4° latitude in width, and the observed values. The medians are about 5% lower than the observations for much of the region between 32° and 68°N latitude, which includes most of the United States and Canada. Again, the IQRs of the model values are about 10% of the median values. As noted earlier, the observations used here are based on measurements at 1200 UTC only. Because the 1200 UTC zonal mean values

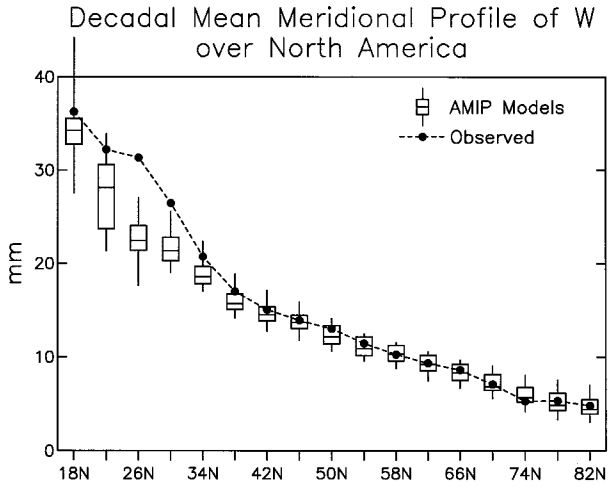

FIG. 3. Decadal and zonal mean distribution of *W* over North America as observed (circles) and the distribution of 28 modeled values (box plots).

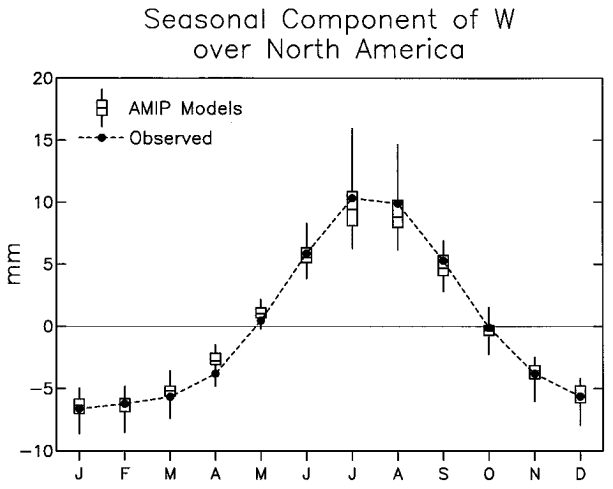

FIG. 4. Climatological seasonal component of *W* averaged over North America as observed (circles) and the distribution of 28 modeled values (box plots).

are, on average, about 1.5% lower than the 0000 UTC values, it is likely that the low bias we find in the models compared with the 1200 UTC data (Fig. 3) is an underestimate of the true bias.

South of 32°N, over Mexico, the models tend to be drier than is observed by as much as 28%, as anticipated by Fig. 1c. We note that the models with high horizontal resolution tend to produce lower simulated *W* values over Mexico than low-resolution models, perhaps because the high-resolution models better represent the high topography, while the radiosonde stations tend to be in lower elevation, coastal locations (Fig. 1a).

c. Seasonal cycle

Over North America the climatological seasonal cycle of precipitable water is readily apparent. The radiosonde observations indicate that summer (JJA) continental-average *W* reaches 23.9 mm, compared with 9.0 mm in winter (DJF). These extreme season values are not symmetric about the annual average of 15.2 mm; the summer departure from the annual average is larger than the winter departure. This asymmetry is consistent with the fairly constant relative humidity from month to month over North America (Gaffen et al. 1992b; Ross and Elliott 1996a), so that *W* increases roughly exponentially with temperature according to the Clausius–Clapeyron relation.

Figure 4 shows the climatological seasonal component of *W* over North America, defined, for each model and for the observations, by the twelve monthly mean *W* values for the decade minus the annual mean *W* for the decade, to remove biases among the latter (Fig. 2). The median values from the models are quite close to the observed, differing by no more than 1.1 mm for any given month.

A noticeable difference between the models and observations is that the models tend to become moister in spring more quickly than the atmosphere, but in the summer the models' medians are drier than observed. This tendency is consistent with a possible systematic error in GCMs' land surface parameterizations, namely, excessive evaporation in spring and insufficient evaporation in summer (P. Viterbo 1996, personal communication; Viterbo and Beljaars 1995).

Most of the models are in good agreement, but some model values are significant outliers. The IQRs and the full ranges of the model values are typically less than 1.5 and 4.5 mm, respectively, except during July and August when they are about twice as large.

One might expect model biases in *W* to be seasonally consistent, that is, that models that are overly dry in summer would also be biased dry in winter. Examining the seasonal model values in more detail, we note a distinct lack of association, however, between the summer and winter *W* values, as shown in Fig. 5. The nonparametric Spearman rank correlation coefficient (Wilks 1995) between JJA and DJF *W* values for the models is an insignificant -0.03. This result suggests that the model biases are not simply related to model architecture but are somehow linked to the treatment of physical processes that vary seasonally, such as convection, evaporation, and precipitation. We examine this possibility in more detail later.

The range of the seasonal cycle of *W* over North America, defined as the difference between the summer and winter mean climatological *W* values, is 14.9 mm in the radiosonde observations, as shown in Fig. 6. Model values range from 10.5 to 21.3 mm, but the median model value, 14.1 mm, is remarkably close to the observed. The observed peak of the seasonal cycle occurs in July, and the minimum is in January (Fig. 4). More than three-quarters of the models correctly simulate this measure of the phase of the seasonal cycle. The rest

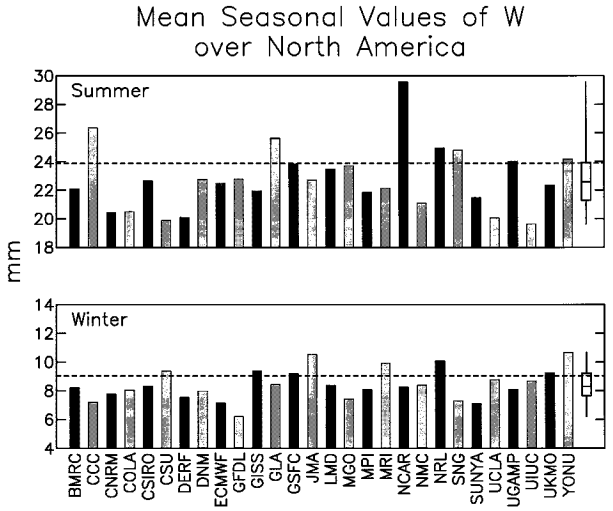

FIG. 5. Climatological summer (JJA, top) and winter (DJF, bottom) values of *W* over North America for each model and as observed (horizontal dashed lines). The box plots give the distribution of model values.

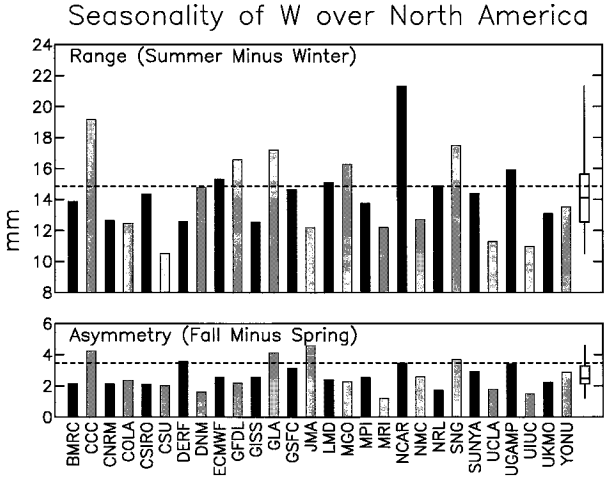

FIG. 6. The summer-minus-winter range of the climatological seasonal cycle of *W* over North America (top) and its fall-minus-spring asymmetry (bottom) from 28 models and as observed (horizontal dashed lines). The box plots give the distribution of model values.

have a maximum or minimum, or both, one month later than is observed, which is a small error given the closeness of the observed January and February values and of the observed July and August values (Fig. 4).

Beyond the asymmetry of the summer and winter *W* values from the annual average, there is an additional asymmetry in the climatological seasonal cycle related to differences between spring and fall; that is, the spring (MAM) and fall (SON) *W* values tend to resemble those of their preceding seasons (DJF and JJA, respectively) more than the following ones (Figs. 4 and 6). This asymmetry of atmospheric water vapor for the equinoctial seasons has been noted previously by Peixoto et al. (1981) over the Northern Hemisphere. The sense of this asymmetry is consistent with the thermal lag of the oceans in the Northern Hemisphere, but, because the North American *W* data show similar asymmetry, the phenomenon is not limited to ocean regions. A tendency for seasonal cyclone totals and their distribution over the continent to show a similar lag relationship was noted by Changnon et al. (1995). The radiosonde observations for North America show a 3.5-mm difference in *W* between fall and spring, which is about 23% of the summer minus winter range. As shown in Fig. 6, each model shows a positive difference as well, although typically the models underestimate this asymmetry by about 30%, which is consistent with the overly rapid moistening of the models in spring noted above.

d. Interannual variability of precipitable water

Although some climatic forcings of the AMIP decade, including the eruption of El Chichón in 1982, were not incorporated in the AMIP simulations, the models were forced by observed sea ice and sea surface temperatures, so there is reason to expect that they will have captured some of the interannual variability of the atmosphere during that decade. Even if all external climate forcings had been incorporated, we would not expect the models' interannual variations to match those of the atmosphere completely because interannual predictability is low outside the Tropics (e.g., Stern and Miyakoda 1995). Model simulations contain variability associated with randomness and a predictable component, which are impossible to separate in a single run. An ensemble of runs with different initial conditions is needed (e.g., Barnett 1995; Stern and Miyakoda 1995).

Nevertheless, swings in the Southern Oscillation, which are related to anomalies of sea surface temperature in the tropical Pacific, are associated with anomalous precipitation (Ropelewski and Halpert 1989) and temperature (Halpert and Ropelewski 1992) patterns over parts of the globe, including parts of North America. Because of the links between temperature, precipitation, and precipitable water, the Southern Oscillation index (SOI) and *W* might also be associated in some regions.

We find, however, that the observed continental mean *W* anomaly time series (Fig. 7) is not correlated at a statistically meaningful level with a time series of the SOI (Ropelewski and Jones 1987; extended), whether monthly, seasonal, or annual anomaly values are used. (In each case, the number of degrees of freedom used to calculate statistical significance was $n - 2$, where n is the number of elements in the 10-yr time series. This choice is based on the very low autocorrelation in the *W* anomaly time series, as discussed below.) As an aside, we note that when longer monthly time series (for 1973–93) of *W* (Ross and Elliott 1996a,b) and SOI are used, we find a significant but small negative correlation between them.

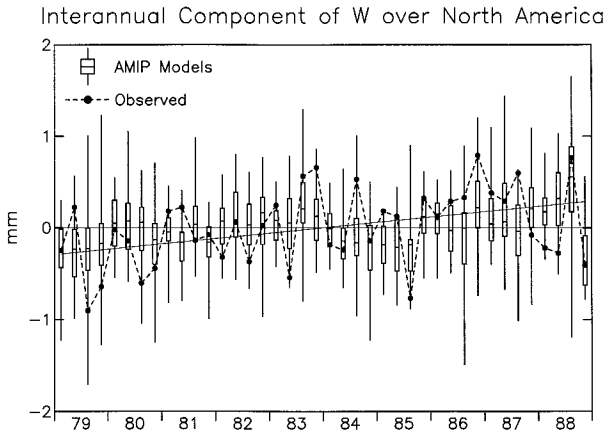

FIG. 7. Distribution of seasonal anomalies of *W* over North America from 28 models (box plots) and as observed (circles). The linear trend of the observed anomalies is also shown.

The observed anomaly time series is also poorly correlated with the simulated time series for the AMIP decade. As shown in Fig. 7, it is not uncommon for most individual models to have seasonal anomalies of opposite sign to the observed. For 23 of the 28 models, the correlation *r* between the model and observed seasonal anomaly time series is not significantly different from zero at the 95% confidence level (*r* exceeding about 0.31). The maximum *r* value is 0.48 for the UKMO model, with the time series based on the median of the 28 models obtaining the next highest *r* value of 0.42.

Having assessed correlations between modeled and observed monthly, annual, and individual season time series, we find that, overall, time series based on the median of the models perform considerably better than almost all models. This result indicates that a ''consensus'' of the models is better related to the variability in the observations than are individual models. The variance of the models' median seasonal anomaly time series is, however, only about 20% of the observed value of 0.17 mm^2, whereas all the individual model simulations have seasonal anomaly variances comparable to the observed. Such a reduction in variance is what would be expected from combining a population of 28 randomly distributed time series. These two results can be interpreted as follows: the median of the 28 model runs captures some of the predictable component of the variability of *W* but is missing some of the random component.

We note that the observations are marked by a trend of 0.55 mm $decade^{-1}$ (Fig. 7), based on linear regression. This linear trend explains 15% of the total variance of the time series. [For a more thorough analysis of North American humidity trends over a longer period, see Ross and Elliott (1996a).] All but four of the models also show a positive trend in *W* over North America, although only 10 of the 24 positive trends are significantly different from 0, on the basis of being more than twice the standard deviation of the trend estimate. The time series based on the median anomalies has a statistically significant trend of 0.25 mm $decade^{-1}$.

Despite the trends, neither the observed nor the models' time series of *W* anomalies over North America shows substantial autocorrelation. For monthly time series, the observed lag-one autocorrelation is 0.16, which is not significant at the 95% confidence level (*r* exceeding about 0.19). The median lag-one autocorrelation for the models is only slightly higher: 0.30. At longer lags the autocorrelations are not significant. For the seasonal time series, the comparable lag-one autocorrelation for the observations is 0.06 and the median from the models is 0.15, neither exceeding 0.30, the 95% confidence level value.

e. Precipitable water, evaporation, and precipitation

The major source of water vapor in the troposphere is evaporation *E* from the surface, and its main sink is precipitation *P*. Although the focus of this study is water vapor, we also examined the AMIP *P* and *E* fields to see whether the differences among model *W* fields might be related to these other components of the hydrological cycle. Lau et al. (1995, Figs. 2 and 3) found that, globally, models with high rates of evaporation have high rates of precipitation. Because atmospheric water vapor is the link between *E* and *P*, one could hypothesize that models with high *E* and *P* also have high *W*.

Using rank correlation analysis, we found no significant relationships, however, between model simulations of decadal mean *W* over North America and either *P* or *E* fields over the continent. We also tested the association between *W* over North America and both *P* and *E* upstream over the North Pacific Ocean and, again, found no significant correlation. On the other hand, rank correlations between *E* and *P* are 0.75 over North America and 0.82 over the North Pacific. Thus, we find, and we infer from the results of Lau et al. (1995), that, both globally and regionally, models with high rates of evaporation tend to have high rates of precipitation. They do not, however, necessarily have high *W*. This result may seem counterintuitive, but we should recall that *P* is more directly related to relative humidity than to *W*, and temperature differences among models could be playing an important role in determining differences in *W*. Evaporation and precipitation rates are indicative of the vigor of the hydrologic cycle and, thus, the mean residence time of water vapor, not its absolute amount.

4. Humidity over the Pacific Ocean

As a counterpoint to the analysis over North America, we considered part of the Pacific basin, between 150°E and 130°W and between 60°N and 60°S, to compare the models over a homogeneous water surface. Radiosonde data are sparse over this region, but satellite-derived estimates of *W* from the Special Sensor Microwave/

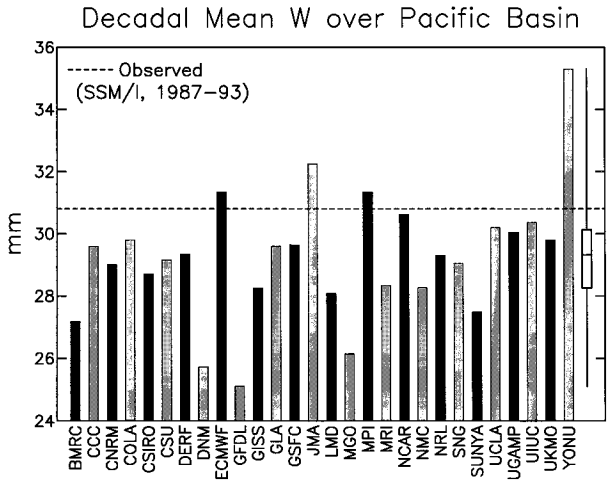

FIG. 8. Decadal mean *W* over the Pacific basin (60°N to 60°S, 150°E to 130°W) for each model (bars) and the distribution of the model values (box plot). The horizontal dashed line indicates the observed value for the period 1987–93 from SSM/I data.

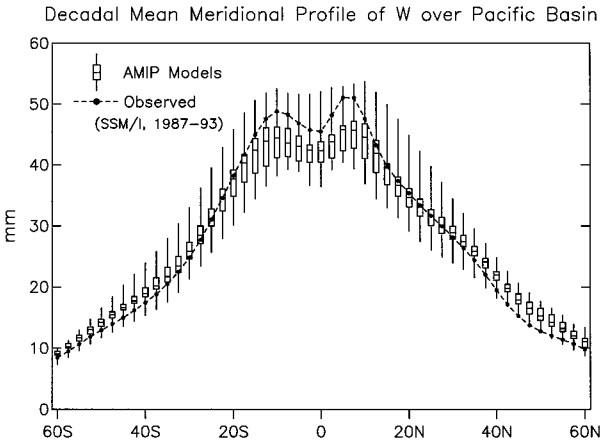

FIG. 9. Meridional profile of *W* over the Pacific basin as observed (circles) and modeled (box plots).

Imager (SSM/I) instrument for the period 1987–93 (Alishouse et al. 1990) provide a useful alternate estimate of the climatological *W* fields. Because there are only 2 yr of overlap between the SSM/I data period and the AMIP decade, we limit our discussion to the climatological fields.

Figure 8 shows the Pacific basin average, decadal mean *W* from each of the 28 models and as estimated from the SSM/I data. The observed and model median *W* values are 30.8 and 29.3 mm, respectively, a difference of 5%. For the models, the ratio of the IQR to the median is 6%, which, although smaller than the 10% value found over North America, is still notable, suggesting that the specification of sea surface temperature is not sufficient to produce identical oceanic *W* fields. We should not expect that *W* in models be a strict function of local sea surface temperatures because other variables, such as tropospheric temperature, lapse rate, and relative humidity, which are related to large-scale dynamics, influence oceanic *W* (Gaffen et al. 1992a; Bony and Duvel 1994). The reduced spread among the models over the sea compared with the continent might be due to model differences in resolving topography, as we discuss in the next section.

The zonal mean values of *W*, shown in Fig. 9, reveal that the underestimates of *W* over the Pacific basin are the result of underestimates between 20°S and 20°N, where the median model values are up to 10% smaller than the SSM/I observations. It is likely, moreover, that the SSM/I *W* retrievals used here are biased low. Jackson and Stephens (1995) found that the Alishouse et al. (1990) SSM/I *W* values are larger than colocated radiosonde-derived values at midlatitudes but smaller than the radiosonde values in the Tropics. The SSM/I data we are using have been adjusted to remedy this bias partially (Colton and Poe 1994), but a low bias in the Tropics probably remains (R. Ferraro 1995, personal communication). An additional bias of unknown magnitude is related to the difference between the period of the SSM/I data record (1987–93) and the AMIP decade (1979–88). Duvel et al. (1997) made a direct comparison of *W* from 10 AMIP models with satellite data for the period 1985–88, and they also found a dry bias in the Tropics. Thus, we conclude that the models are substantially drier than the real atmosphere over the tropical Pacific basin; however, unlike over North America, we cannot point to orography differences between models and observations as a factor contributing to the bias.

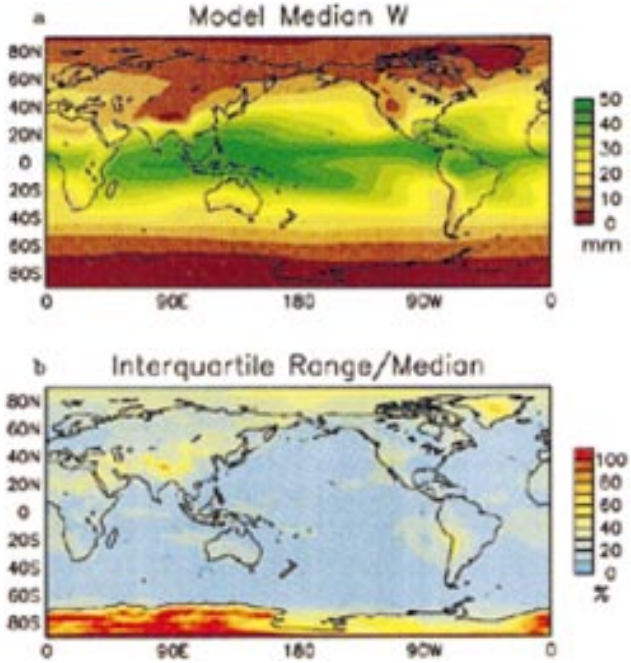

FIG. 10. (a) Median values and (b) the ratio of the interquartile range to the median of 28 model simulations of the decadal mean *W* over the globe.

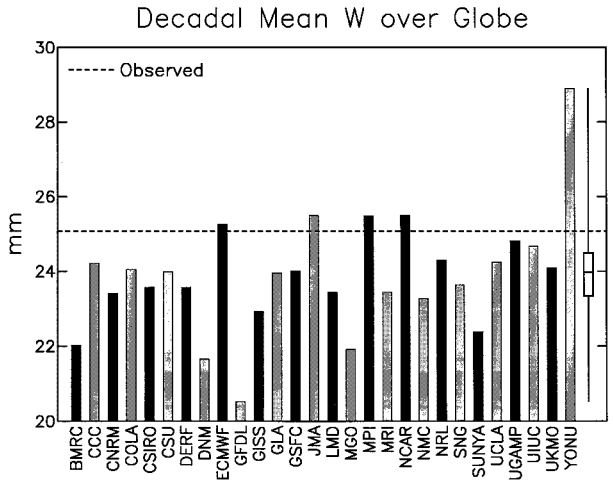

FIG. 11. Globally integrated decadal-mean W for each model (bars) and the distribution of the model values (box plot). The horizontal dashed line indicates the value observed for the same decade based on analyses of radiosonde observations by Oort (1983).

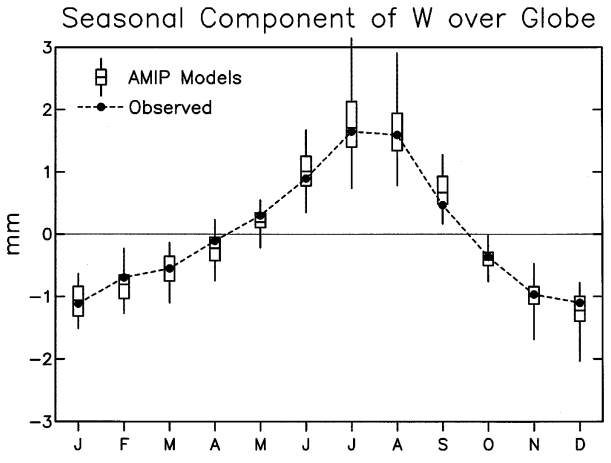

FIG. 12. Climatological seasonal component of globally integrated W as observed (circles) and the distribution of model values (box plots).

5. Global precipitable water and meridional moisture flux

Broadening our coverage to the global scale, Fig. 10a depicts the median of the 28 AMIP models' simulations of W over the globe. The expected features of the global W climatology are evident, including the general decrease of W from the equator poleward, low W values over high terrain and known desert regions, and maximum W over the tropical Pacific warm pool.

The global map of the ratio of the IQR to the median (Fig. 10b) shows that this measure of the intermodel variability of the W simulations is between 10% and 20% over most of the world's oceans and over low elevation continental regions. Over high terrain, the ratio is generally between 40% and 80%. It appears, therefore, that the variation in how models resolve topographic features is the main source of disparity among model simulations of climatological W fields. The exceptionally large ratios, exceeding 100%, over Antarctica are also related to very low W values there (Fig. 10a).

The global- and decadal-mean values of W for each of 28 AMIP models and their distribution are shown in Fig. 11. For comparison, we also present the global- and decadal-mean W computed using gridded analyses of the 0000 and 1200 UTC radiosonde observations during 1979–88 produced by Oort (1983) and Oort and Liu (1993). Monthly mean fields of q on a $2.5° \times 5°$ latitude–longitude grid at individual pressure levels have been integrated between the surface and 300 hPa to produce global W maps, from which global averages were calculated.

Although these analyses suffer from well-known problems associated with the irregular distribution of radiosonde stations across the globe, they nevertheless represent the most comprehensive and homogeneous source of upper-air global circulation statistics currently available for the AMIP period. Those analyses of W based on fields from analysis-forecast systems are problematic because such analyses can depend considerably on the architecture of a particular system, which, moreover, typically changes with time (Trenberth and Guillemot 1995). Atmospheric reanalyses, which are beginning to become available (e.g., Kalnay et al. 1996), may be useful for future studies, although differences among reanalyses from different modeling centers will have to be reconciled.

Evident in Fig. 11 is a tendency for the model atmospheres to be drier than observed over the globe, as found over North America and the tropical Pacific Ocean. We note, however, that estimates of the total precipitable water over the globe, $\{W\}$, vary considerably, although the value reported here based on the Oort analyses (25.1 mm) lies well within the range of other observations, as summarized by Wittmeyer and Vonder Haar (1994). In any case, the model median $\{W\}$ is some 4.4% (1.1 mm) smaller than the observed value, and nearly one-fifth of the model values are more than 10% smaller than observed.

The IQR is 4.8% of the median model value, which is smaller than the comparable statistics over North America or the Pacific basin. On the other hand, the IQR is comparable to the amount by which $\{W\}$ would increase during two decades of global warming, assuming a warming of 0.7 K and no appreciable changes in relative humidity (Del Genio 1993). The current discrepancy among GCMs in simulating $\{W\}$ for the AMIP decade is, therefore, of consequence for interpreting GCM predictions of climate change.

Despite such difficulties in reproducing the decadal-mean $\{W\}$, it is reassuring to discover (Fig. 12) that the models can produce reasonable seasonal variations in $\{W\}$, as they were observed to do over North America (Fig. 4). The global seasonal cycle has the signature of

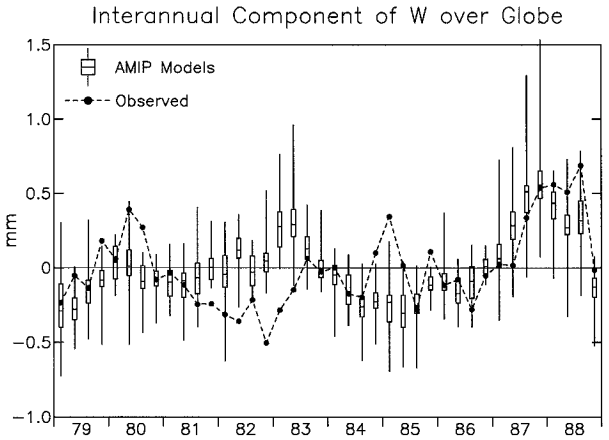

FIG. 13. Distribution of seasonal anomalies of globally integrated *W* from 28 models (box plots) and as observed (circles).

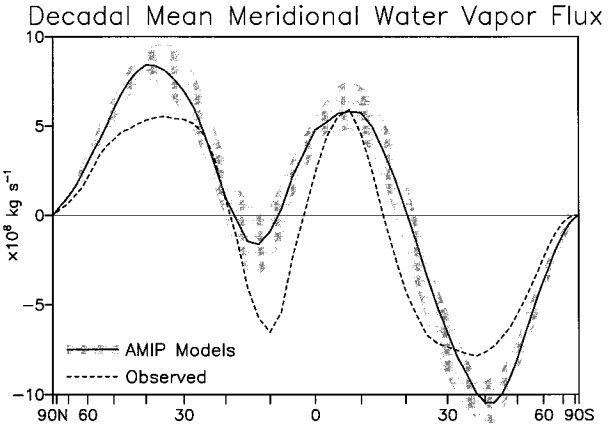

FIG. 14. The median (solid line) of the 28 model profiles of the total meridional flux of water vapor, $2\pi a \cos(\phi)\,[Q_\phi]$ (where a is the earth's radius and ϕ is latitude), as inferred from water vapor budget considerations. The shaded area indicates the interquartile range of model values. Positive values indicate northward fluxes. The observed value is also shown (dashed line).

the Northern Hemisphere where *W* peaks in summer. The tendency for a larger range of model values during northern summer deserves further investigation.

Interannual variations in the models' {*W*} values (Fig. 13) are marked by an ENSO signal. The correlation between the median of the models' seasonal {*W*} anomaly time series and seasonal values of the SOI (Ropelewski and Jones 1987; extended) is −0.42, significant at the 99% confidence level. The extension to a domain beyond North America here appears to incorporate the influence of warm sea surface temperatures in the eastern tropical Pacific on modeled {*W*}. The reality of this signal is difficult to confirm with the available observations, although Jackson and Stephens (1995) find an El Niño–Southern Oscillation signal in *W* integrated over the global oceans from SSM/I measurements during July 1987–June 1991. On the other hand, Sun and Oort (1995) and Soden and Lanzante (1996) note problems in capturing this signal properly with the radiosonde network alone because of the poor data coverage in the eastern Pacific. Perhaps as a result the correspondence between the observed and model median curves in Fig. 13 is less than ideal ($r = 0.47$), and the correlation ($r = 0.17$) between the observations and SOI values is not significant.

Because it is important to the global energy and water cycle, we consider briefly the large-scale flux of moisture over the globe. Figure 14 shows profiles of the net meridional transport of water vapor for the AMIP decade. The model profiles have been deduced from the archived AMIP standard output of evaporation, precipitation, and *W;* however, the observed profile of this transport has been determined directly from Oort's analyses of meridional vapor fluxes through evaluating the relationship $[Q_\Phi] = \int [qv]\, dp$ (where v is the meridional wind component, p is pressure from the surface to 300 hPa, and the square brackets denote zonal mean values). The figure reveals a clear tendency for the models to overestimate systematically the poleward flux of moisture (and latent heat) over much of the globe, although uncertainties in the observations are potentially large and need to be taken into account. Interestingly, Gleckler et al. (1995) find that the AMIP models also tend to overestimate the poleward total atmospheric energy transport; the results in Fig. 14 suggest that as much as 50% or more of this bias may be accounted for by excessive moisture fluxes.

6. Potential sources of model differences

To determine the possible reasons for the spread among the model simulations of precipitable water (and other hydrological variables), we measured the association between several aspects of the models' formulations, as summarized by Phillips (1994), and their simulations of decadal mean *W, P,* and *E* over North America and the Pacific basin and of global *W.* We also considered possible associations between model formulations and the net meridional moisture flux but in a much more limited fashion.

The 14 facets of model formulation considered are given in the top row of Table 2. Two of these are the models' horizontal and vertical resolution, and, as numerical quantities, they were rank correlated with the hydrological variables tested, which are summarized in the first column of Table 2.

The remaining 12 variables are dichotomous. For example, a model either does or does not contain prescribed soil moisture fields. For the characteristics described by dichotomous variables, the table shows the number of models with that characteristic. We note that only in the case of soil moisture schemes does the number of models in the three categories sum to 28. The two model characteristics associated with the planetary boundary layer are independent, as are the two asso-

TABLE 2. Relationships between aspects of GCM formulation and the tendencies in simulated precipitable water (W) and evaporation (E) and precipitation (P) rates. Statistically significant relationships are indicated according to whether the model characteristic is associated with higher or lower values of the variable in question, otherwise a dash appears. (Note that in the case of Northern Hemisphere moisture flux, only relationships with model spatial resolution were tested.)

	Spatial resolution		Planetary boundary layer		Numerics		Convective scheme				Soil moisture scheme			Reevaporation of precipitation
	Vertical	Horizontal	Prognostic PBL depth	Vertical diffusion above PBL	Finite difference	Moisture filling	Moist convective adjustment	Interactive cumulus subensembles	Moisture convergence closure	Bulk mass flux	Bucket	Prescribed	Vegetation	
Number of models	—	—	3	21	10	20	5	8	7	5	20	4	4	17
North America W	—	—	—	—	—	—	—	—	—	—	low	high	—	—
Pacific basin W	—	—	—	—	—	low	—	—	—	—	—	—	—	—
Global W	—	—	—	—	—	low	—	—	—	—	—	—	—	—
North America E	—	—	high	low	—	—	—	high	—	—	—	high	—	—
North America P	—	low	high	—	—	—	—	—	low	—	—	—	—	—
Pacific basin E	—	—	high	—	—	—	—	—	—	—	—	—	—	—
Pacific basin P	—	—	high	—	—	—	—	—	—	—	—	—	—	—
Northern Hemisphere moisture flux	—	—												

ciated with numerics. The convective schemes include the possibility of hybrid approaches (for which a model would fall into more than one category) but do not include all approaches used in the AMIP models.

We used the Student's *t* test to determine whether the group of models with a given characteristic have mean values of simulated hydrologic variables that are significantly different from the mean of the remaining models. The results of these tests are summarized in Table 2. If a *t* test shows the difference in the means to be significant at the 95% confidence level or better, or if the rank correlation is significant at that level, the table shows whether the model characteristic is associated with higher or lower values of the variable in question.

We stress that finding an explanation for the relationships revealed is not straightforward and may be impossible because of the complexity of the GCMs. Determining the effects of different model characteristics by comparing various GCMs may be impossible. Controlled experiments in which characteristics are changed one at a time may be needed to determine the sensitivity of a particular model to particular aspects of its construction.

Furthermore, the model properties we examined are interrelated. For example, models using convective schemes with interactive cumulus subensembles are often offsprings of the UCLA model and so share other traits as well. Thus, the models are not independent in a statistical sense, and a relationship among them might have nothing to do with the convective scheme but another aspect(s) of their construction.

a. Vertical and horizontal resolution

Model vertical resolution, measured as the total number of vertical levels, shows no significant correlation with any of the variables tested. Models with high horizontal resolution have low *P* over North America. We find little association between model horizontal resolution (as measured by the total number of grid points globally) and *W* except, as noted before, that high resolution models simulate lower *W* over Mexico than low resolution models. As noted above, we suspect that differences in model horizontal resolution account for the high intermodel variability noted in regions of high terrain (Fig. 10b).

Our result differs from those of Phillips et al. (1995) and Williamson et al. (1995), who found tendencies for total precipitable water in the ECMWF and NCAR models, respectively, to decrease with increasing horizontal resolution, although for the ECMWF model the effect was most pronounced in the Tropics and was not monotonic. Our result that the peak northward flux of moisture in the Northern Hemisphere is insensitive to horizontal resolution differs from that of Manabe et al. (1991), who report that this flux decreased with increasing horizontal resolution in their version of the GFDL model.

b. Planetary boundary layer formulation

In three of the models, the depth of the planetary boundary layer is a prognostic variable, rather than a fixed value. Because the boundary layer contains a large fraction of the total column *W* and because mixing of water vapor from the boundary layer to the free troposphere is limited by atmospheric stability, we would expect that the depth of the boundary layer will have a strong influence on *W*. The models with prognostic boundary layers tend to have high *E* and high *P* over both North America and the Pacific basin but there is no significant association with *W*. The use of schemes

to allow the vertical diffusion of moisture above the planetary boundary layer in 21 of the models is associated with low North American *E* values but with no other tendencies in the simulated moisture variables shown in Table 2.

c. Numerical approaches

The application of finite-difference numerical schemes or spectral methods to solve the governing equations has no particular impact on the variables examined. The use of moisture filling techniques to eliminate spurious negative values of humidity is associated with low *W* values over the Pacific basin and globally.

d. Method of parameterizing convection

To examine the relationship between the parameterization of atmospheric convection and simulated hydrological variables, we considered four broad categories of models. We caution that some models use hybrid approaches so that a model might fall into more than one category. In addition, the parameterization of atmospheric convection is a complex matter, and because each approach is sensitive to the details of implementation (e.g., Bony et al. 1995) and to other related GCM parameterizations, categorizing models in this way is an oversimplification.

Five of the 28 models employ moist convective adjustment schemes (e.g., Manabe et al. 1965), and the *t* tests show no significant differences between this group and the remaining 23 models. Eight models employ convective schemes with interactive cumulus subensembles (e.g., Arakawa and Schubert 1974), and they tend to have high *E* over North America.

Seven models parameterize convection based on moisture convergence closure (e.g., Kuo 1974), and they are associated with low *P* over North America. The use of bulk mass flux schemes (e.g., Tiedtke 1989) in five models has no significant association with the simulated *W*, *E*, or *P* examined. Direct comparison of the models using bulk mass flux and moisture convergence closure schemes showed no significant differences. This finding differs from the results of Colman and McAvaney (1995) who found that a mass flux convective scheme produced a moister troposphere in the BMRC model than did a moisture convergence convective scheme.

e. Soil moisture

Following the classification developed by Robock et al. (1995) for the treatment of soil moisture in the AMIP GCMs, we tested the association between *W* and use of 1) ''bucket'' models in 20 GCMs, 2) prescribed soil moisture in four GCMs, and 3) soil moisture schemes involving vegetation models in four GCMs.

Bucket models tend to be associated with low *W* over North America, and models with prescribed soil moisture tend to have high North American *W* and *E* values. The models incorporating vegetation show no particular tendencies with respect to *W, E,* or *P*.

f. Evaporation from falling precipitation

Seventeen models allow for the reevaporation of moisture from falling precipitation, which one might expect to enhance tropospheric water vapor. Our analysis shows no significant differences, however, between these 17 models and the remaining 11.

g. Can we explain model differences?

The most striking aspect of Table 2 is the large fraction of cells that are blank; the number of filled cells is not large, although it is higher than what would be expected by chance. The useful information in Table 2 is where there are consistent tendencies in different hydrological variables, such as is seen with prognostic PBL depth. Nevertheless, overall, and in agreement with the results of Weare et al. (1995), who studied AMIP total cloudiness simulations, the statistical results presented here do not point to obvious connections between specific aspects of model architecture and simulated hydrological variables.

7. Conclusions

Comparisons of observations and 28 AMIP simulations of tropospheric water vapor show the following.

1) The models tend to underestimate the decadal mean precipitable water by approximately 5% over North America and globally as compared with radiosonde observations, and over the Pacific basin as compared with satellite SSM/I observations.
2) The largest disparity among models' decadal mean *W* fields occurs over regions of high terrain, probably because of differences in resolving topography. Over North America, the relatively high elevation in the models compared to the radiosonde network is a partial explanation for the dry bias of the models as a group. There is no significant correlation, however, between the individual models' mean elevation and their mean *W* values, and topography is clearly not the source of the dry bias over the Pacific basin.
3) The mean seasonal cycles of precipitable water are reasonably well simulated but with a wide range among models.
4) The models do not capture much of the observed interannual variability in precipitable water. Overall, a consensus of the models, as defined by the median of the 28 models considered, gives a better simulation of the observed interannual variability than do individual models.
5) The models appear to overestimate the poleward flux of moisture, which probably contributes to the gen-

eral overestimate of atmospheric poleward energy flux found by other investigators.

6) There is little association between aspects of model formulation and simulated hydrological variables. A more fruitful approach would probably involve controlled experiments with individual GCMs, in which one aspect of the model is changed systematically and the impact on the simulations is assessed. Such an approach is currently under consideration as part of a successor to AMIP, AMIP II, which could also involve multiple simulations from each participating model to extract the predicted interannual signal from random noise and would better specify the boundary conditions and forcing functions for the period of simulation.

Acknowledgments. We are especially grateful to the AMIP modeling groups and the Program for Climate Model Diagnosis and Intercomparison at Lawrence Livermore National Laboratory for making the simulations available for this project. We thank Rebecca Ross of NOAA for preparing the North American radiosonde dataset used in this study and Peter Nelson of AER, Inc., for dealing with the global-scale datasets and for preparing the figures. We also thank William Elliott, Sharon LeDuc, Peter Stone, Peter Rowntree, Pedro Viterbo, and two anonymous reviewers for their helpful comments. The work at AER, Inc., was partially supported by the Climate Dynamics Program of the National Science Foundation under Grant ATM-9223164 and by the U.S. Department of Energy's National Institute for Global Environmental Change, through the NIGEC Northeast Regional Center at Harvard University (DOE Cooperative Agreement DE-FC03-90ER61010).

REFERENCES

Alishouse, J. C., S. A. Snyder, J. Vongasthorn, and R. R. Ferraro, 1990: Determination of oceanic precipitable water from the SSM/I. *IEEE Trans. Geosci. Remote Sens.,* **28,** 811–816.

Arakawa, A., and W. H. Schubert, 1974: Interaction of a cumulus cloud ensemble with the large-scale environment. Part I. *J. Atmos. Sci.,* **31,** 674–701.

Barnett, T. P., 1995: Monte Carlo climate forecasting. *J. Climate,* **8,** 1005–1022.

Bony, S., and J.-P. Duvel, 1994: Influence of the vertical structure of the atmosphere on the seasonal variation of precipitable water and greenhouse effect. *J. Geophys. Res.,* **99,** 12 963–12 980.

——, ——, and H. Le Treut, 1995: Observed dependence of the water vapor and clear-sky greenhouse effect on sea surface temperature: Comparison with climate warming experiments. *Climate Dyn.,* **11,** 307–320.

Boyle, J., 1993: Sensitivity of dynamical quantities to horizontal resolution for a climate simulation using the ECMWF (cycle 33) model. *J. Climate,* **6,** 796–815.

Changnon, D., J. J. Noel, and L. H. Maze, 1995: Determining cyclone frequencies using equal-area circles. *Mon. Wea. Rev.,* **123,** 2285–2294.

Chen, C.-T., E. Roeckner, and B. J. Soden, 1996: A comparison of satellite observations and model simulations of column-integrated moisture and upper-tropospheric humidity. *J. Climate,* **9,** 1561–1585.

Colman, R. A., and B. J. McAvaney, 1995: Sensitivity of the climate response of an atmospheric general circulation model to changes in convective parameterization and horizontal resolution. *J. Geophys. Res.,* **100,** 3155–3172.

Colton, R. A., and G. A. Poe, 1994: Shared Processing Program, Defense Meteorological Satellite Program, Special Sensor Microwave/Imager Algorithm Symposium, 8–10 June 1993. *Bull. Amer. Meteor. Soc.,* **75,** 1663–1669.

Del Genio, A., 1993: Accuracy requirements. Long-term monitoring of global climate forcings and feedbacks. NASA Conf. Publ. 3234, 91 pp. [Available from NASA Center for Aerospace Information, 800 Elkridge Landing Road, Linthicum Heights, MD 21090-2934.]

——, W. Kovari Jr., and M-S. Yao, 1994: Climatic implications of the seasonal variation of upper tropospheric water vapor. *Geophys. Res. Lett.,* **21,** 2701–2704.

Duvel, J.-P., S. Bony, and H. LeTreut, 1997: Clear-sky greenhouse effect sensitivity to sea surface temperature changes: An evaluation of AMIP simulations. *Climate Dyn.,* in press.

Elliott, W. P., and D. J. Gaffen, 1991: On the utility of radiosonde humidity archives for climate studies. *Bull. Amer. Meteor. Soc.,* **72,** 1507–1520.

Gaffen, D. J., 1993: Historical changes in radiosonde instruments and practices. WMO/TD-No. 541, Instruments and Observing Methods Rep. 50, 123 pp. [Available from World Meteorological Organization, P.O. Box 2300, CH-1211 Geneva, Switzerland.]

——, 1996: A digitized metadata set of global upper-air station histories. NOAA Tech. Memo. ERL ARL-211, 38 pp. [Available from National Technical Information Service, 5285 Port Royal Road, Springfield, VA 22061.]

——, and T. P. Barnett, 1992: A comparison of observations and model simulation of tropospheric water vapor. *J. Geophys. Res.,* **97,** 2775–2780.

——, W. P. Elliott, and A. Robock, 1992a: Relationships between tropospheric water vapor and surface temperature as observed by radiosondes. *Geophys. Res. Lett.,* **19,** 1839–1842.

——, A. Robock, and W. P. Elliott, 1992b: Annual cycles of tropospheric water vapor. *J. Geophys. Res.,* **97,** 18 185–18 193.

Gates, W. L., 1992: AMIP: The Atmospheric Model Intercomparison Project. *Bull. Amer. Meteor. Soc.,* **73,** 1962–1970.

Gleckler, P. J., and Coauthors, 1995: Cloud-radiative effects on implied oceanic energy transports as simulated by atmospheric general circulation models. *Geophys. Res. Lett.,* **22,** 791–794.

Halpert, M. S., and C. F. Ropelewski, 1992: Surface temperature patterns associated with the Southern Oscillation. *J. Climate,* **5,** 594–614.

Jackson, D. L., and G. L. Stephens, 1995: A study of SSM/I-derived columnar water vapor over the oceans. *J. Climate,* **8,** 2025–2038.

Kalnay, E., and Coauthors, 1996: The NCEP/NCAR 40-year reanalysis project. *Bull. Amer. Meteor. Soc.,* **77,** 437–471.

Kuo, H. L., 1974: Further studies of the parameterization of the influence of cumulus convection on large-scale flow. *J. Atmos. Sci.,* **31,** 1232–1240.

Lau, W. K.-M., Y. C. Sud, and J.-H. Kim, 1995: Intercomparison of hydrologic processes in global climate models. NASA Tech. Memo. 104617, 170 pp. [Available from NASA Center for Aerospace Information, 800 Elkridge Landing Road, Linthicum Heights, MD 21090-2934.]

Manabe, S., J. Smagorinsky, and R. F. Strickler, 1965: Simulated climatology of a general circulation model with a hydrologic cycle. *Mon. Wea. Rev.,* **93,** 769–798.

——, R. J. Stouffer, M. J. Spelman, and K. Bryan, 1991: Transient responses of a coupled ocean–atmosphere model to gradual changes of atmospheric CO_2. Part I: Annual mean response. *J. Climate,* **4,** 785–818.

Oort, A. H., 1983: Global Atmospheric Circulation Statistics, 1958–1973. NOAA Prof. Paper 14, 180 pp. and 47 microfiche. [Avail-

able from National Technical Information Service, 5285 Port Royal Road, Springfield, VA 22161.]

——, and H. Liu, 1993: Upper-air temperature trends over the globe, 1958–1989. *J. Climate,* **6,** 292–307.

Peixoto, J. P., D. A. Salstein, and R. D. Rosen, 1981: Intra-annual variation in large-scale moisture fields. *J. Geophys. Res.,* **86,** 1255–1264.

Phillips, T. J., 1994: A summary documentation of the AMIP models. PCMDI Rep. 18, UCRL-ID-116384, 343 pp. [Available from National Technical Information Service, U.S. Dept. of Commerce, 5285 Port Royal Rd., Springfield, VA 22161.]

——, L. C. Corsetti, and S. L. Grotch, 1995: The impact of horizontal resolution on moist processes in the ECMWF model. *Climate Dyn.,* **11,** 85–102.

Rind, D., E.-W. Chiou, W. Chu, J. Larsen, S. Oltmans, J. Lerner, M. P. McCormick, and L. McMaster, 1991: Positive water vapor feedback in climate models confirmed by satellite data. *Nature,* **349,** 500–503.

Roads, J. O., S.-C. Chen, J. Kao, D. Langley, and G. Glatzmaier, 1992: Global aspects of the Los Alamos general circulation model hydrological cycle. *J. Geophys. Res.,* **97,** 10 051–10 068.

——, S. Marshall, R. Oglesby, and S.-C. Chen, 1996: Sensitivity of the CCM1 hydrological cycle to CO_2. *J. Geophys. Res.,* **101,** 7321–7339.

Robock, A., C. A. Schlosser, K. Ya. Vinnikov, S. Liu, and N. Speranskaya, 1995: Validation of humidity, moisture fluxes, and soil moisture in GCMs: Report of AMIP diagnostic subproject 11: Part 1-Soil Moisture. *Proc. First AMIP Scientific Conference,* Monterey, CA, World Meteorological Organization, 85–90.

Ropelewski, C. F., and P. D. Jones, 1987: An extension of the Tahiti–Darwin Southern Oscillation index. *Mon. Wea. Rev.,* **115,** 2161–2165.

——, and M. S. Halpert, 1989: Precipitation patterns associated with the high index phase of the Southern Oscillation. *J. Climate,* **2,** 268–284.

Ross, R. J., and W. P. Elliott, 1996a: Tropospheric water vapor climatology trends over North America: 1973–93. *J. Climate,* **9,** 3561–3574.

——, and ——, 1996b: Tropospheric precipitable water: A radiosonde-based climatology. NOAA Tech. Memo. ERL ARL-219, 132 pp. [Available from National Technical Information Service, 5285 Port Royal Road, Springfield, VA 22061.]

Salathé, E. P., Jr., D. Chesters, and Y. C. Sud, 1995: Evaluation of the upper-tropospheric moisture climatology in a general circulation model using TOVS radiance observations. *J. Climate,* **8,** 2404–2414.

Soden, B. J., and F. P. Bretherton, 1994: Evaluation of water vapor distribution in general circulation models using satellite observations. *J. Geophys. Res.,* **99,** 1187–1210.

——, and J. R. Lanzante, 1996: Satellite and radiosonde climatologies of upper tropospheric water vapor. *J. Climate,* **9,** 1235–1250.

Srinivasan, G., M. Hulme, and C. G. Jones, 1995: An evaluation of the spatial and interannual variability of tropical precipitation as simulated by GCMs. *Geophys. Res. Lett.,* **22,** 2139–2142.

Stern, W., and K. Miyakoda, 1995: Feasibility of seasonal forecasts inferred from multiple GCM simulations. *J. Climate,* **8,** 1071–1085.

Sun, D.-Z., and A. H. Oort, 1995: Humidity–temperature relationships in the tropical troposphere. *J. Climate,* **8,** 1974–1987.

Thompson, S. L., and D. Pollard, 1995: A global climate model (GENESIS) with a land-surface transfer scheme (LSX). Part I: Present climate simulation. *J. Climate,* **8,** 732–761.

Tiedtke, M., 1989: A comprehensive mass flux scheme for cumulus parameterization in large-scale models. *Mon. Wea. Rev.,* **117,** 1779–1800.

Trenberth, K. E., and C. J. Guillemot, 1995: Evaluation of the global atmospheric moisture budget as seen from the analyses. *J. Climate,* **8,** 2255–2772.

Tukey, J. W., 1977: *Exploratory Data Analysis.* Addison-Wesley, 688 pp.

Viterbo, P., and A. C. M. Beljaars, 1995: An improved land surface parameterization in the ECMWF model and its validation. *J. Climate,* **8,** 2716–2748.

Weare, B. C., and Coauthors, 1995: Evaluation of total cloudiness and its variability in the Atmospheric Model Intercomparison Project. *J. Climate,* **8,** 2224–2238.

Wilks, D. S., 1995: *Statistical Methods in the Atmospheric Sciences.* Academic Press, 467 pp.

Williamson, D. L., J. T. Kiehl, and J. J. Hack, 1995: Climate sensitivity of the NCAR Community Climate Model (CCM2) to horizontal resolution. *Climate Dyn.,* **11,** 377–397.

Wittmeyer, I. L., and T. H. Vonder Haar, 1994: Analysis of the global ISCCP TOVS water vapor climatology. *J. Climate,* **7,** 325–333.